Inorganic Chemistry
Article

Inorg. Chem. **2010**, *49*, 10809–10814 **10809**
DOI: 10.1021/ic1011007

Crystal Structures and Magnetic Properties of New Europium Melilites $Eu_2MSi_2O_7$ (M = Mg, Mn) and Their Strontium Analogues

Takashi Endo,* Yoshihiro Doi, Makoto Wakeshima, and Yukio Hinatsu

Division of Chemistry, Graduate School of Science, Hokkaido University, Sapporo 060-0810, Japan

Received June 1, 2010

Synthesis, crystal structures, and magnetic properties of melilite-type oxides $A_2MSi_2O_7$ (A = Sr, Eu; M = Mg, Mn) were investigated. These compounds crystallize in the melilite structure with space group $P\bar{4}2_1m$. The ^{151}Eu Mössbauer measurements show that the Eu ions are in the divalent state. The $Eu_2MgSi_2O_7$ is paramagnetic down to 1.8 K. Long-range antiferromagnetic ordering is observed at 3.4 K for $Sr_2MnSi_2O_7$. On the other hand, the $Eu_2MnSi_2O_7$ shows a ferrimagnetic transition at 10.7 K. From the magnetization and specific heat measurements, it is found that the Eu^{2+} (14 μ_B) and Mn^{2+} (5 μ_B) sublattices order antiferromagnetically. This result indicates that an interaction between f-d electrons (Eu−Mn) predominantly operate in this compound.

1. Introduction

The melilite-type oxides have the general formula $A_2MM'_2O_7$ (A = larger cations such as alkali earth ions and lanthanides; M, M′ = smaller divalent to tetravalent cations). Many of them crystallize in a tetragonal structure with space group $P\bar{4}2_1m$, and this structure can be described as a two-dimensional network consisting of MO_4 and $M'O_4$ tetrahedra in the *ab*-plane and larger A ions located between these networks.[1−3] For this structural feature, magnetic properties of $A_2MM'_2O_7$ compounds (A = Ca, Sr, Ba; M = Mn, Co, Cu; M′ = Si, Ge) have been attracting interest. They show anomalous behaviors derived from the two-dimensional arrangement of magnetic M ions. For example, $Ba_2MnGe_2O_7$ behaves as a square lattice Heisenberg antiferromagnet (T_N = 4.0 K),[4] and $Ba_2CuGe_2O_7$ has a spiral spin structure below 3.26 K.[5] Two compounds $A_2CoSi_2O_7$ (A = Ca, Sr) show both antiferromagnetic and dielectric anomalies, and are regarded as new candidates for multiferroic materials.[6] On the other hand, the melilite-type oxides in which the magnetic ions fully occupy the A site are very few. Among them, $A_2GeBe_2O_7$ (A = Pr, Sm, Gd, Dy, and Er) are paramagnetic down to 5 K.[3,7]

To explore further interesting materials, we have paid our attention to the melilites containing magnetic ions in both A (= lanthanides) and M (= transition metals) sites. Such compounds are expected to show magnetic behavior, reflecting both d-d interactions and f-d interactions. To our best knowledge, however, no previous investigations were carried out.

In this study, we investigated the syntheses, crystal structures, and magnetic properties of new Eu-containing melilites $Eu_2MnSi_2O_7$ (M = Mg, Mn). Because the ionic radius of Eu^{2+} is very close to that of Sr^{2+}, it should be possible to prepare such compounds. The results of the powder X-ray diffraction (XRD), ^{151} Mössbauer spectrum, magnetic susceptibility, and specific heat measurements are discussed.

2. Experimental Procedures

2.1. Synthesis. Polycrystalline samples (0.5 g) of $A_2MSi_2O_7$ (A = Sr, Eu; M = Mg, Mn) were prepared by the standard solid-state reaction. For starting materials, SrO, Eu_2O_3, MgO, MnO, SiO_2, and Si were used. Before use, Eu_2O_3 and MgO were heated at 900 °C overnight. The SrO was prepared by the decarbonation of $SrCO_3$ at 1400 °C for 12 h. These starting materials were weighed out in a stoichiometric ratio and well mixed in an agate mortar. The mixtures were pressed into pellets and wrapped in a molybdenum foil, and then they were sealed in evacuated quartz tubes. These ampules were heated at 1100 °C for 36−48 h.

2.2. XRD Analysis. Powder XRD measurements were performed at room temperature using a Multi-Flex diffractometer (Rigaku) with a Cu Kα X-ray radiation source equipped with a curved graphite-monochromator. The data were collected by step-scanning in the angle range of $10° \leq 2\theta \leq 120°$ at a step size

*To whom correspondence should be addressed. Phone: +81-11-706-2702. Fax: +81-11-706-4931. E-mail: t-endo38232@mail.sci.hokudai.ac.jp.

(1) Burzo, E. *Melilites and related silicates in Landolt-Börnstein, New Series Vol.3/27 i2*; Springer: Berlin, 2005.
(2) Kaninskii, A. A.; Bohaty, L.; Becker, P.; Liebertz, J.; Held, P.; Eichler, H. J.; Rhee, H.; Hanuza, J. *Laser Phys. Lett.* **2008**, *5*(12), 845–868.
(3) Mill, B. V.; Baibakova, G. D. *Russ. J. Inorg. Chem.* **1990**, *35*(3), 341–343.
(4) Masuda, T.; Kitaoka, S.; Takamizawa, S.; Metoki, N.; Kaneko, K.; Rule, K. C.; Kiefer, K.; Manaka, H.; Nojiri, H. *Phys. Rev. B.* **2010**, *81*, 100402(R).
(5) Zheludev, A.; Shirane, G.; Sasago, Y.; Kiode, N.; Uchinokura, K. *Phys. Rev. B.* **1996**, *54*(21), 15163–15170.
(6) Akaki, M.; Tozawa, J.; Akahoshi, D.; Kuwahara, H. *J. Phys.: Conf. Ser.* **2009**, *150*, 042001.
(7) Ochi, Y.; Morikawa, H.; Marumo, F.; Nozaki, H. *Yogyo - Kyokai - Shi* **1983**, *91*(5), 229–234.

Published on Web 10/29/2010

0.02°. The XRD data were analyzed by the Rietveld method using the program RIETAN-FP,[8] and the crystal structures were drawn by VESTA program.[9]

2.3. ^{151}Eu Mössbauer Spectroscopy Measurements. The ^{151}Eu Mössbauer spectra were measured at room temperature with a Mössbauer VT - 6000 transmission spectrometer (Laboratory Equipment) using a radiation source $^{151}SmF_3$(1.85 GBq). The spectrometer was calibrated with α-iron at room temperature, and the isomer shift (I.S.) was determined relative to the shift of europium trifluoride (EuF_3). The γ-ray was detected by a NaI scintillation counter. The powdered sample was wrapped in an aluminum foil (1.5 cm ×1.5 cm) with the density of 15 mg (Eu)/cm^2.

2.4. Magnetic Measurements. The temperature dependence of the magnetic susceptibilities was measured with a SQUID magnetometer (Quantum Design, MPMS-5S). The measurements were performed under both zero-field-cooled (ZFC) and field-cooled (FC) conditions over the temperature range 1.8−300 K in an applied magnetic field of 0.1 T. The field dependence of the magnetizations was measured with a commercial physical property measurement system (Quantum Design, PPMS) over the magnetic field range between −9 and 9 T at 1.8 K.

2.5. Specific Heat Measurements. The specific heat measurements were performed using a relaxation technique with the PPMS in the temperature range of 1.8−300 K. The pelletized sample was mounted on a thin alumina plate with Apiezon N-grease for better thermal contact.

2.6. Calculation of the Quadrupole Coupling Constant. The calculation of the quadrupole coupling constant was carried out by the WIEN2k program using the full potential linearized augmented plane wave + local orbitals (FP-LAPW + lo) method based on the density functional theory (DFT) with the generalized gradient approximation (GAA).[10]

3. Result and Discussion

3.1. Crystal Structure. The melilite-type oxides $Sr_2MSi_2O_7$ (M = Mg, Mn) and their new analogues $Eu_2MSi_2O_7$ (M = Mg, Mn) were successfully prepared. They were obtained as white (A = Sr) or light-green (Eu) colored polycrystalline samples. The trial to synthesize other $Eu_2MSi_2O_7$ compounds (M = Fe, Co, Ni, Cu) ended in failure because the M^{2+} ion was reduced to the metal by the introduction of the Eu^{2+} ion (the major products were M metal and apatite-type oxides $Eu_5Si_3O_{13}$).

The XRD profiles for $Sr_2MnSi_2O_7$ and $Eu_2MnSi_2O_7$ are shown in Figure 1. The observed peaks were indexed on a tetragonal unit cell ($a \sim 8$ Å, $c \sim 5$ Å) with the space group $P\bar{4}2_1m$, which is typical for the melilite-type compounds.[1,2] Among the compounds prepared in this study, only the $Sr_2MnSi_2O_7$ contains a small amount of $SrSiO_3$ (∼ 1%) as an impurity. The XRD data were analyzed by the Rietveld method using the structural parameters of $Sr_2MgSi_2O_7$ as a starting model.[11] The calculated profiles are also plotted in Figure 1. The refined structural parameters and reliability factors are summarized in Table 1.

The schematic crystal structure of the title compounds is illustrated in Figure 2, and some selected interatomic distances of A−O, M−O, and Si−O are listed in Table 2. In this structure, both the M and Si ions are coordinated by four oxygen ions, forming MO_4 and SiO_4 tetrahedra, respectively. These MO_4 and SiO_4 tetrahedra are linked by sharing corner-oxygen ions, and thus they build a two-dimensional layer consisting of five-membered rings in the *ab*-plane. Beneath these rings, the A ions are located in the eight-coordinated sites, forming another layer. These two kinds of layers are alternately stacked along the *c*-axis. In the AO_8 polyhedron, there are six kinds of A−O distances between 2.54 Å and 2.83 Å, and its shape is highly distorted. Reflecting almost the same ionic radii between Sr^{2+} (1.26 Å) and Eu^{2+} (1.25 Å),[12] these six distances are very close among four compounds in Table 2. The bond valence sums (BVS)[13,14] are calculated from the interatomic distances, and they are also listed in Table 2. These values indicate that the A and M ions are in the divalent state and the Si ion is in the tetravalent state.

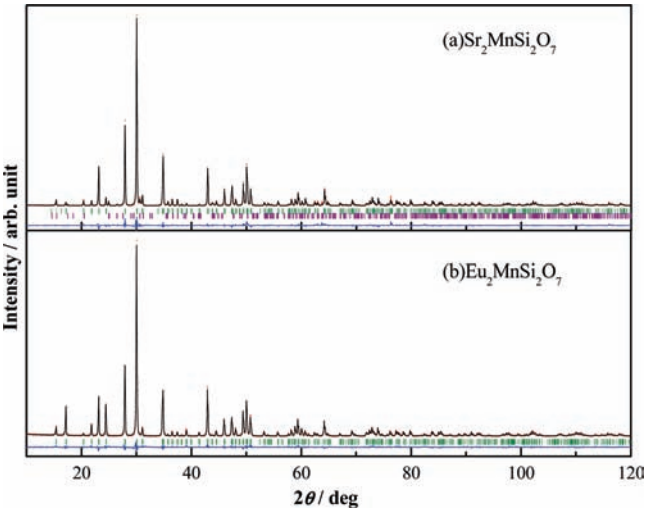

Figure 1. Powder XRD profiles for (a) $Sr_2MnSi_2O_7$ and (b) $Eu_2MnSi_2O_7$. The calculated and observed profiles are shown on the top black solid line and red cross markers, respectively. The vertical marks in the middle show positions calculated for Bragg reflections. The lower trace is a plot of the difference between calculated and observed intensities. For (a), the second vertical marks show an impurity phase ($SrSiO_3$).

Table 1. Structural Parameters for $A_2MnSi_2O_7$ (A = Sr, Eu)

atom	site	*x*	*y*	*z*	*B*(Å^2)
		$Sr_2MnSi_2O_7$[a]			
Sr	4*e*	0.3333(1)	0.1667	0.5068(2)	0.82(1)
Mn	2*a*	0	0	0	0.51(4)
Si	4*e*	0.1361(2)	0.3639	0.9399(4)	0.50(1)
O1	2*c*	1/2	0	0.1420(1)	0.92(7)
O2	4*e*	0.1420(5)	0.3580	0.2454(9)	0.92
O3	8*f*	0.0767(4)	0.2007(5)	0.7939(8)	0.92
		$Eu_2MnSi_2O_7$[b]			
Eu	4*e*	0.3342(1)	0.1658	0.5055(2)	0.37(2)
Mn	2*a*	0	0	0	0.54(6)
Si	4*e*	0.1366(3)	0.3634	0.9422(7)	0.30(1)
O1	2*c*	1/2	0	0.1421(1)	0.30(1)
O2	4*e*	0.1432(7)	0.3568	0.2501(1)	0.30
O3	8*f*	0.0791(6)	0.1946(7)	0.7980(1)	0.30

[a] Space group $P\bar{4}2_1m$ (No. 113), Z=2, a = 8.1315(1) Å, c = 5.1589(1) Å, R_{wp} = 9.22%, R_p = 6.80%, R_e = 2.99%, R_I = 1.90%. [b] Space group $P\bar{4}2_1m$ (No. 113), Z=2, a = 8.1390(2) Å, c = 5.1635(1) Å, R_{wp} = 9.87%, R_p = 7.05%, R_e = 7.52%, R_I = 2.28%.

(8) Izumi, F.; Momma, K. *Solid State Phenom.* **2007**, *130*, 15–20.
(9) Momma, K.; Izumi, F. *J. Appl. Crystallogr.* **2008**, *41*, 653–658.
(10) Blaha, P.; Schwarz, K.; Madsen, G. K.; Kvasnicka, D.; Luitz, J. *WIEN2k, An augmented Plane Wave Plus Local Orbitals Programs for Calculating Crystal properties*; 2001.
(11) Kimata, M. *Z. Kristallogr.* **1983**, *163*, 295–304.
(12) Shannon, R. D. *Acta. Crystallogr.* **1976**, *A32*, 751–767.
(13) Brown, I. D.; Altermatt, D. *Acta Crystallogr., Sect B.* **1985**, *B41*, 244–247.

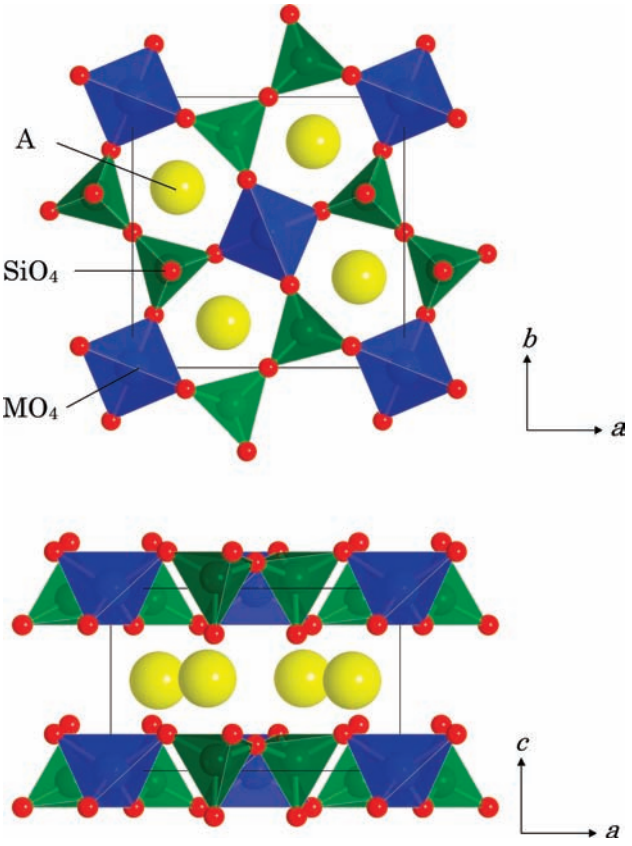

Figure 2. Schematic crystal structure of melilite-type oxides $A_2MSi_2O_7$ (A = Sr, Eu; M = Mg, Mn). (a) Viewed from the *c*-axis, (b) projection of the structure in the *ac*-plane.

Table 2. Selected Interatomic Distances (Å) and Bond Valence Sums Determined by X-ray Diffraction Measurements

	$Sr_2MgSi_2O_7$	$Sr_2MnSi_2O_7$	$Eu_2MgSi_2O_7$	$Eu_2MnSi_2O_7$
A−O2	2.582(5)	2.580(5)	2.542(7)	2.565(7)
A−O3 × 2	2.588(4)	2.573(4)	2.572(6)	2.579(6)
A−O1	2.606(1)	2.686(5)	2.634(7)	2.679(7)
A−O2′ × 2	2.749(4)	2.825(4)	2.736(5)	2.820(6)
A−O3′ × 2	2.792(4)	2.736(4)	2.802(5)	2.780(5)
BVS (A^{2+})	1.80	1.76	1.77	1.87
M−O3	1.945(3)	2.045(54)	1.947(5)	2.002(5)
BVS (M^{2+})	2.05	2.01	2.01	2.26
Si−O2	1.573(5)	1.577(5)	1.640(8)	1.590(8)
Si−O3 × 2	1.594(3)	1.600(4)	1.602(5)	1.630(5)
Si−O1	1.624(3)	1.622(3)	1.619(4)	1.631(4)
BVS (Si^{4+})	4.29	4.25	4.07	4.03

3.2. ^{151}Eu Mössbauer Spectrum. Figure 3 shows the ^{151}Eu Mössbauer spectra for $Eu_2MgSi_2O_7$ and $Eu_2MnSi_2O_7$ at room temperature. In both spectra, an absorption peak appears at about 13 mm/s, indicating the presence of the divalent Eu ions. On the other hand, no absorption peak was observed at 0.5−1 mm/s corresponding to the trivalent Eu ion.[15] Therefore, the Eu ions in both compounds are in the divalent state. The observed peak is strongly asymmetric because of the quadrupole interaction. The quadrupole Hamiltonian is given by

$$H_Q = \frac{e^2qQ}{4I(2I-1)}\left(3I_z^2 - I(I+1) + \eta(I_x^2 + I_y^2)\right) \qquad (1)$$

(14) Brese, N. E.; O'Keeffe, M. *Acta Crystallogr., Sect B.* **1991**, *B47*, 192–197.
(15) *Mössbauer Spectroscopy Applied to Inorganic Chemistry* ; Long, G. J., Grandjean, F., Eds.; Plenum Press: New York, 1986; Vol. *3*, p545.

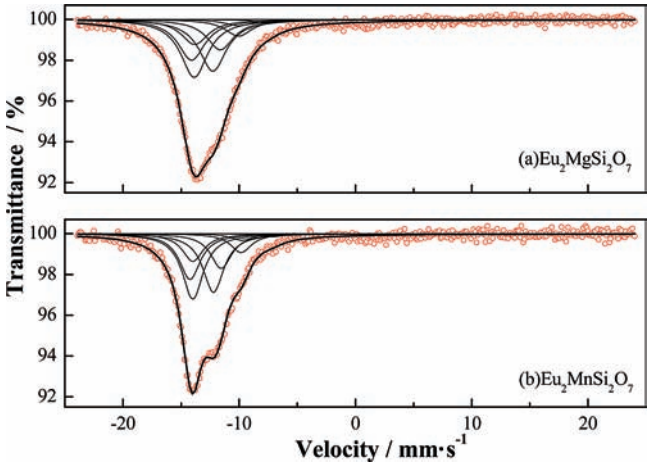

Figure 3. Mössbauer spectra for (a) $Eu_2MgSi_2O_7$ and (b) $Eu_2MnSi_2O_7$. The observed spectra are shown on the red circles.

Table 3. Mössbauer Parameters for $Eu_2MSi_2O_7$ (M = Mg, Mn)

compound	I.S. (mm/s^{-1})	Q.S. (mm/s^{-1})	η	Γ(mm/s^{-1})
$Eu_2MgSi_2O_7$	−12.81(1)	−13.65(2)	0.26(3)	2.82(4)
$Eu_2MnSi_2O_7$	−12.84(5)	−14.91(4)	0.29(4)	2.19(4)

where I is the nuclear spin, Q is the quadrupole moment, $eq = V_{ZZ}$, and $\eta = (V_{XX} - V_{YY})/V_{ZZ}$ (V_{ii} is the electric field gradient tensor). The 12 possible transitions (eight allowed transitions and four forbidden transitions) due to a quadrupole interaction were taken into account; the observed data were fitted with the sum of these Lorenzian lines. To derive these Lorenzian equations, the results by Shenoy and Dunlap were used, and the ratio of the excited and ground state quadrupole moments ($R_Q = Q_e/Q_g$) was taken as 1.312.[16,17] The fitting curves are shown in Figure 3, and determined fitting parameters are listed in Table 3.

The large Q.S. (−13 ∼ −15 mm/s) and non-zero η (∼0.3) values indicate that the Eu ion is in a greatly distorted coordination environment in these compounds. In fact, this ion is located in the distorted EuO_8 polyhedron with various Eu−O lengths (Table 2). The Q.S. and η values are also calculated by the electronic structure calculation using the structural parameters for $Eu_2MgSi_2O_7$. They ($Q.S._{cal} = -11.1$ mm/s, $\eta_{cal} = 0.46$) are in good agreement with the experimental data, which corresponds to the observed ones. Such a large Q.S. value has been found in $EuZrO_3$ perovskite containing divalent Eu ion (Q.S. = −12.64 mm/s and η = 0.46).[18]

3.3. Magnetic Properties. 3.3.1. $Sr_2MnSi_2O_7$. Figure 4 shows the temperature dependence of the reciprocal magnetic susceptibility for $Sr_2MnSi_2O_7$. The data were fitted by the Curie−Weiss law between 100 and 300 K, using an equation

$$\chi_M = \frac{C}{(T-\theta)} + \chi_{TIP} \qquad (2)$$

(16) Shenoy, G. K.; Dunlap, B. D. *Nucl. Instrum. Methods* **1969**, *71*, 285.
(17) Robinson, J. W. *Handbook of Spectroscopy*; CRC: Boca Raton, FL, 1981; Vol. *3*, p 464 .
(18) Zong, Y.; Fujita, K.; Akamatsu, H.; Murai, S.; Tanaka, K. *J. Solid State Chem.* **2010**, *183*, 168–172.

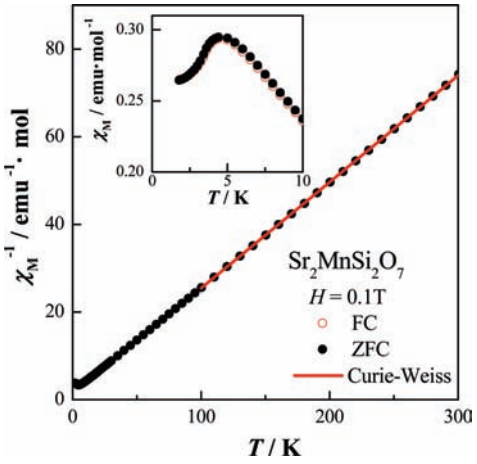

Figure 4. Temperature dependence of the reciprocal magnetic susceptibility of $Sr_2MnSi_2O_7$. The red-solid line is a result of fit with the Curie−Weiss law. The inset shows the susceptibility versus temperature curve at low temperatures.

where C, θ, and χ_{TIP} mean the Curie constant, Weiss constant, and temperature independent paramagnetic susceptibility, respectively. The effective magnetic moment (μ_{eff}) and Weiss constant were determined to be 5.78(3) μ_B/*f.u.* and −6.0(3) K, respectively. The value of μ_{eff} is close to the magnetic moment of 5.92 μ_B for the Mn^{2+} ion in a high-spin configuration ($3d^5$, $S = 5/2$). The negative θ value indicates that the predominant magnetic interaction between Mn ions is antiferromagnetic, and actually an antiferromagnetic transition is observed at ∼4 K (see the inset of Figure 4).

Figure 5 shows the temperature dependence of the specific heat for $Sr_2MnSi_2O_7$. The data show a λ-type anomaly at 3.4 K, indicating the occurrence of the long-range antiferromagnetic ordering of Mn^{2+} ions. The magnetic entropy (S_{mag}) due to the magnetic ordering was calculated from the specific heat data. To evaluate the lattice specific heat (C_{lat}) of $Sr_2MnSi_2O_7$, specific heat data for the nonmagnetic $Sr_2MgSi_2O_7$ were used. However, the specific heat of $Sr_2MgSi_2O_7$ showed a poor fit to the C_p of $Sr_2MnSi_2O_7$ above the magnetic transition temperature. Then, the C_{lat} of $Sr_2MnSi_2O_7$ was obtained from the sum of the Debye and Einstein models:

$$C_{lat} = 9R\left(\frac{T}{\theta_D}\right)^3 \int_0^{\theta_D/T} \frac{(\theta_D/T)^4 e^{\theta_D/T}}{(e^{\theta_D/T}-1)^2} d(\theta_D/T) + R\sum_{i=1}^{3} \frac{(\theta_{E_i}/T)^2 e^{\theta_{E_i}/T}}{(e^{\theta_{E_i}/T}-1)^2} \quad (3)$$

where θ_D is the Debye temperature, and $\theta_{E1} \sim \theta_{E3}$ are the Einstein temperatures.[19] The calculated C_{lat} values are shown as a solid line in Figure 5a. The magnetic specific heat (C_{mag}) was obtained by subtracting the lattice specific heat (C_{lat}) from C_p. Then, the magnetic specific heat was determined by using the equation $S_{mag} = \int_0^T C_{mag}/T \, dT$. The magnetic specific heat below 1.8 K was extrapolated by the relation $C_{mag} \propto T^3$ from the spin-wave model for an antiferromagnet.[20] The temperature dependence of the magnetic specific heat divided by temperature (C_{mag}/T)

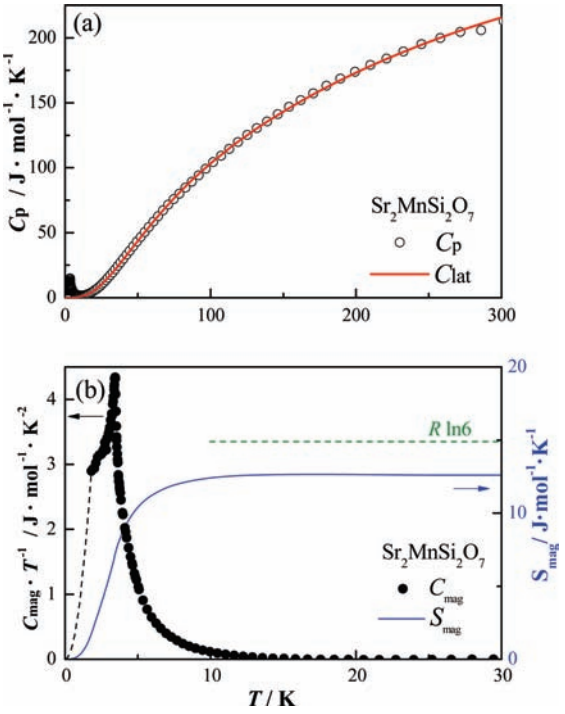

Figure 5. (a) Temperature dependence of specific heat (C_P), and (b) magnetic specific heat divided by temperature ($C_{mag}T^{-1}$) and magnetic entropy (S_{mag}) for $Sr_2MnSi_2O_7$.

and magnetic entropy (S_{mag}) is plotted in Figure 5b. The S_{mag} value reaches 12.5 J mol^{-1} K^{-1} at 100 K, which is close to the theoretical value R ln(2S+1) = R ln 6 = 14.90 J mol^{-1} K^{-1} (R = gas constant). This result shows that the observed magnetic transition is due to the antiferromagnetic ordering of the Mn^{2+} ion in a high-spin configuration (S=5/2).

3.3.2. $Eu_2MgSi_2O_7$. Figure 6 shows the temperature dependence of the reciprocal magnetic susceptibility for $Eu_2MgSi_2O_7$, in which only A site ions (Eu^{2+}) are magnetic. The susceptibility above 100 K was fitted with the Curie−Weiss law (eq 2). The effective magnetic moment and Weiss constant were determined to be 11.02(4) μ_B/*f.u.* and −1.2(4) K, respectively. The μ_{eff} value is in good agreement with the spin-only value (11.23 μ_B) for two Eu^{2+} ions ($S = 7/2$). The small negative Weiss constant may indicate the existence of the antiferromagnetic interaction between Eu ions; however, no magnetic transition is observed down to 1.8 K. The temperature dependence of the specific heat for $Eu_2MgSi_2O_7$ is plotted in Figure 7. Below ∼10 K, the specific heat increases with decreasing temperature, which shows the onset of magnetic ordering of the Eu ions. Figure 8 shows the field dependence of the magnetization for $Eu_2MgSi_2O_7$ measured at 1.8 K. The magnetization (M) increases with magnetic field (H) and shows a saturation behavior. The value of the saturation magnetization (13.2 μ_B) is reasonable for two Eu ions (7 μ_B×2). The observed $M-H$ curve is below the Brillouin curve. Therefore, we fitted the data using a modified Brillouin function:[22]

$$M = gSB_s\left(\frac{g S\mu_B H}{k_B(T-T_0)}\right) \quad (4)$$

(19) Grimvall, G. *Thermophysical Properties of Materials in Selected topics in solid state physics*; Elsevier/North-Holland: New York, 1986; Vol. *13*, pp 65−115.
(20) Joshua, S. J.; Cracknell, A. P. *Phys. Rev. Lett.* **1969**, *A28*, 562–563.
(21) Zielinski, M.; Rigaux, C.; Lemaître, A.; Deportes, J. *Phys. Rev. B.* **1996**, *53*(2), 674–685.
(22) Néel, L. *Ann. Phys. Paris.* **1948**, *3*, 133–198.

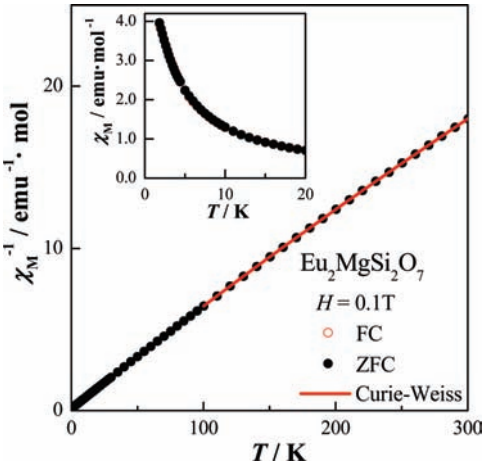

Figure 6. Temperature dependence of the reciprocal magnetic susceptibility of $Eu_2MgSi_2O_7$. The red-solid line is a fitting result by the Curie−Weiss law. The inset shows the susceptibility versus temperature curve at low temperatures.

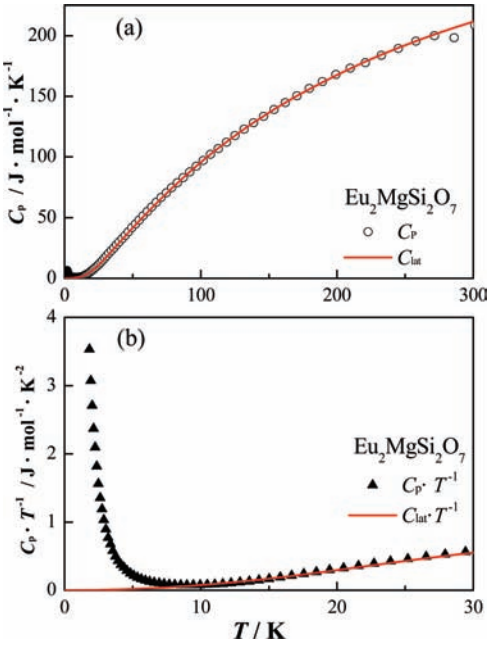

Figure 7. (a) Temperature dependence of specific heat (C_P) and (b) specific heat divided by temperature ($C_{mag}T^{-1}$) at the low temperature range for $Eu_2MgSi_2O_7$.

where parameter T_0 accounts phenomenologically for the magnetic interaction between Eu^{2+} ions. The fitting curve is shown in Figure 9. The negative value of T_0 (−1.0 K) agrees with the Weiss constant (−1.2 K), and it indicates that the ground state of $Eu_2MgSi_2O_7$ is antiferromagnetic.

3.3.3. $Eu_2MnSi_2O_7$. Figure 9 shows the temperature dependence of the reciprocal magnetic susceptibility for $Eu_2MnSi_2O_7$. In this compound, both the A and M sites are occupied by magnetic ions, that is, Eu^{2+} ($4f^7$) and Mn^{2+} ($3d^5$), respectively. The effective magnetic moment determined from the data above 100 K is 12.32(1) $\mu_B/f.u.$, which is in good agreement with the calculated value $\mu_{eff} = (2(\mu_{Eu^{2+}} + \mu_{Mn^{2+}})^{1/2} = 12.69\ \mu_B$ from the paramagnetic moments of Eu^{2+} ($S = 7/2$) and Mn^{2+} ($S = 5/2$) ions. The negative Weiss constant (−29.5(2) K) suggests

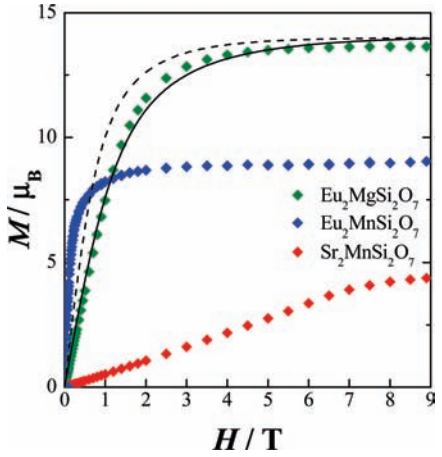

Figure 8. Field dependence of the magnetization curve of $A_2MSi_2O_7$ compounds measured at 1.8 K. The black dashed and solid lines are the normal and modified Brillouin functions with $S = 7/2$. (see text) There are no hysteresis loops in all the data.

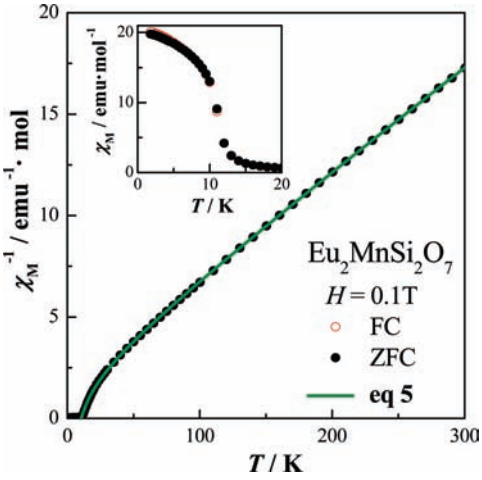

Figure 9. Temperature dependence of the reciprocal magnetic susceptibility of $Eu_2MnSi_2O_7$. The green-solid line is a fitting curve by eq 5 (see text.). The inset shows the susceptibility versus temperature curve at low temperatures.

the presence of the antiferromagnetic interaction. However, this compound shows a ferromagnetic-like anomaly below12 K.

To obtain furthermore information about this magnetic behavior, specific heat measurements were carried out. The specific heat C_p data (Figure 10a) show a λ-type anomaly at 10.7 K, indicating the occurrence of the long-range magnetic ordering. The magnetic specific heat C_{mag} is calculated by subtracting the lattice specific heat C_{lat} (eq 3) from the C_p data. In a similar way to the case for $Sr_2MnSi_2O_7$, the C_{lat} data were estimated from the sum of the Debye and Einstein models. The total magnetic entropy change (Figure 10b) is 43.5 J mol^{-1} K^{-1} at 100 K, which is close to the value 49.48 J mol^{-1} K^{-1} expected from the sum of $2R$ ln 8 for Eu^{2+} and R ln 6 for Mn^{2+}. Therefore, this magnetic transition is due to the magnetic ordering of both Eu and Mn ions.

The negative Weiss constant may indicate that the observed magnetic transition is attributed to a ferrimagnetic ordering rather than a ferromagnetic one. According to the molecular field theory, the temperature

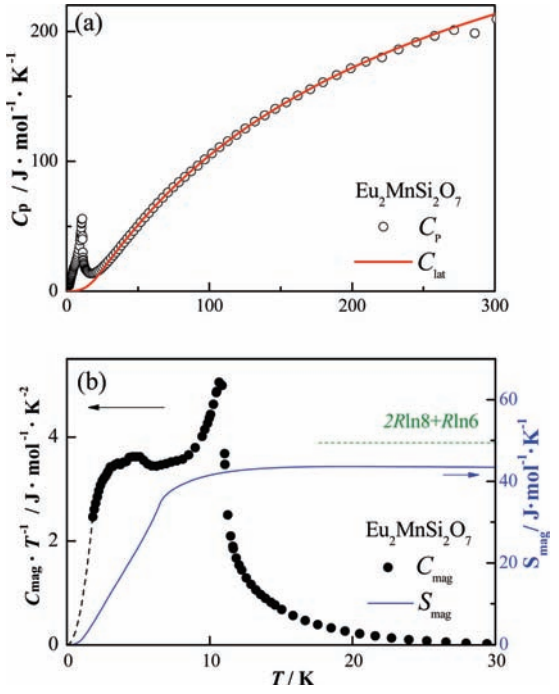

Figure 10. (a) Temperature dependence of specific heats divided by temperature (C_pT^{-1}) and (b) the magnetic specific heat divided by temperature ($C_{mag}T^{-1}$) and magnetic entropy (S_{mag}) for $Eu_2MnSi_2O_7$.

dependence of the reciprocal magnetic susceptibility for a ferrimagnet is represented by

$$\frac{1}{\chi - \chi_{TIP}} = \frac{T}{C} + \frac{1}{\chi_0} - \frac{\sigma}{T - \theta} \quad (5)$$

where the parameters χ_0, θ, and σ are related to the molecular field magnetic coefficients.[21] For $Eu_2MnSi_2O_7$, the Curie temperature T_C {$= (\theta - C/\chi_0 + [(\theta - C/\chi_0)^2 + 4C(\theta/\chi_0 + \sigma)]^{1/2})/2$} and the Curie constant C ($= C_{Eu} + C_{Mn}$) are determined to be 10.69(1) K and 18.99(4) emu K mol^{-1}, respectively, by fitting eq 4 to the $\chi_M^{-1} - T$ curve as shown in Figure 9. The T_C value agrees with the temperature at which magnetic susceptibility and specific heat measurements show an anomaly (10.7 K).

The field dependence of the magnetization for $Eu_2MnSi_2O_7$ measured at 1.8 K is also shown in Figure 8. The magnetization increases quickly with magnetic field and shows a saturation behavior. The saturation magnetization ~9.0 μ_B is much smaller than the value 19 μ_B expected from the fully ferromagnetic ordering of both Eu^{2+} (7 μ_B × 2) and Mn^{2+} sublattices (5 μ_B) and rather close to 9 μ_B for a ferrimagnetic ordering between sublattices.

3.3.4. Magnetic Interaction in $A_2MSi_2O_7$ (A = Sr, Eu; M = Mg, Mn). From the magnetic measurements of $Sr_2MnSi_2O_7$, an antiferromagnetic ordering of Mn^{2+} ions is observed at 3.4 K. The interatomic distances of Mn ions are 5.75 Å ($= a/\sqrt{2}$) in the *ab*-plane and 5.16 Å ($= c$) along the *c*-axis (see Figure 2 and Table 1). Recently, the exchange integral $|J|$ values for two interaction pathways in the analogous compound $Ba_2MnGe_2O_7$ (T_N = 4.0 K) were determined by the inelastic neutron scattering experiment: 27.8 μeV (the Mn−Mn distance is 6.01 Å) and 1.0 μeV (5.53 Å), respectively.[4] Thus, it is expected that the antiferromagnetic interaction between Mn−Mn ions in the *ab*-plane is predominant also in $Sr_2MnSi_2O_7$. On the other hand, the experimental results on $Eu_2MgSi_2O_7$ indicate that the magnetic interaction between A sites (Eu^{2+} ions) is also antiferromagnetic. Nevertheless, $Eu_2MnSi_2O_7$ shows a ferrimagnetic transition at 10.7 K. The data of specific heat and magnetization measurements are explained well by the antiparallel arrangement of the Eu and Mn sublattices, that is, the ferromagnetic Eu^{2+} (14 μ_B) layer and ferromagnetic Mn^{2+} (5 μ_B) layer, in contrast to the expected antiferromagnetic Mn−Mn and Eu−Eu interactions, are alternately stacked along the *c*-axis. In this structure, the interatomic distance between Eu and Mn ions is 3.97−4.00 Å, which is shorter than those of Mn−Mn ions (5.74 Å) and Eu−Eu ions (4.29 Å). This result indicates that an antiferromagnetic interaction between Eu and Mn ions is predominant in this compound.

4. Conclusions

We here report synthesis, crystal structures, and magnetic properties of quaternary compounds $A_2MSi_2O_7$ (A = Sr, Eu, M = Mg, Mn). They crystallize in a tetragonal melilite-type structure with space group $P\bar{4}2_1m$. The ^{151}Eu Mössbauer spectrum measurements show that the Eu ions are in the divalent state in these compounds. $Sr_2MnSi_2O_7$ shows an antiferromagnetic transition at 3.4 K. On the other hand, $Eu_2MnSi_2O_7$ shows a ferrimagnetic transition at 10.7 K.

Acknowledgment. This research was partially supported by the Global COE Program (Project No. B01: Catalysis as the Basis for Innovation in Materials Science) from Ministry of Education, Culture, Sports, Science and Technology.

Supporting Information Available: Figure S1, Powder X-ray diffraction profiles for (a) $Sr_2MgSi_2O_7$ and (b) $Eu_2MgSi_2O_7$. Table S1, Structural parameters for $A_2MgSi_2O_7$ (A = Sr, Eu). Crystallographic data in CIF format. This material is available free of charge via the Internet at http://pubs.acs.org.